Astrophysics of CAI formation as revealed by silicon isotope LA-MC-ICPMS of an igneous CAI

Anat Shahar [a,*], Edward D. Young [a,b]

[a] Department of Earth and Space Sciences, University of California Los Angeles, United States
[b] Institute of Geophysics and Planetary Physics, University of California Los Angeles, United States

Abstract

Silicon isotope ratios of a typical CAI from the Leoville carbonaceous chondrite, obtained *in situ* by laser ablation MC-ICPMS, together with existing $^{25}Mg/^{24}Mg$ data, reveal a detailed picture of the astrophysical setting of CAI melting and subsequent heating. Models for the chemical and isotopic effects of evaporation of the molten CAI are used to produce a univariant relationship between P_{H_2} and time during melting. The result shows that this CAI was molten for a cumulative time of no more than 70 days and probably less than 15 days depending on temperature. The object could have been molten for an integrated time of just a few hours if isotope ratio zoning was eliminated after melting by high subsolidus temperatures (e.g., >1300 K) for ∼500 yr. In all cases subsolidus heating sufficient to produce diffusion-limited isotope fractionation at the margin of the solidified CAI is required. These stable isotope data point to a two-stage history for this igneous CAI involving melting for a cumulative timescale of hours to months followed by subsolidus heating for years to hundreds of years. The thermobarometric history deduced from combining Si and Mg isotope ratio data implicates thermal processing in the disk, perhaps by passage through shockwaves, following melting. This study underscores the direct link between the meaning of stable isotope ratio zoning, or lack thereof, and the inferred astrophysical setting of melting and subsequent processing of CAIs.
© 2007 Elsevier B.V. All rights reserved.

Keywords: silicon isotopes; meteorites; CAI; laser ablation

1. Introduction

Isotope cosmobarometry refers to the use of stable isotope fractionation in primitive meteoritical materials as an ambient gas pressure indicator [1]. In this context, we are concerned with estimating the pressures (dominated by H_2) attending igneous calcium–aluminum-rich inclusion (CAI) formation in the early solar system. The partial pressure of H_2 (P_{H_2}) is a key clue to the astrophysical environs of CAI formation in the solar protoplanetary disk. In this paper we demonstrate that Si isotope ratios of a CAI obtained *in situ* by laser ablation multiple-collector inductively coupled plasma-source mass spectrometery (LA-MC-ICPMS) can be used as a cosmobarometer to constrain the thermobarometric history of the object. We show further that comparison of Si and Mg isotope fractionations provides an especially useful way to elucidate the physicochemical environments of CAI formation. The comparison is

* Corresponding author.
E-mail address: ashahar@ess.ucla.edu (A. Shahar).

revealing because while these elements are similar in volatility, their mass-dependent isotope fractionations upon evaporation are distinctive. The results bear on the pressure, temperature, composition, and time path followed by CAIs in the early solar system prior to their incorporation into chondrite parent bodies.

There is a wealth of information about the physical chemistry associated with evaporation and condensation of CAI-like liquids at low pressures. The kinetics of isotope fractionation during condensation and evaporation are also well known. Previous work includes parameterization of the thermodynamics that controls the rates of evaporation of Ca, Al, Mg, and Si from $CaO–Al_2O_3–MgO–SiO_2$ (CMAS) melts and experimental determinations of evaporation factors, γ_i (γ_i relates measured evaporation rates for species i to the evaporation rates predicted by the Hertz–Knudsen equation) [2,3]. With this information it is possible to calculate the extent of Si and Mg isotope fractionation resulting from evaporation of a molten CMAS object in space as a function of pressure, temperature, chemical composition, and time.

It is well known that igneous CAIs tend to have high $^{29}Si/^{28}Si$ and high $^{25}Mg/^{24}Mg$ relative to chondritic values [4], and experimental and computational data have been used previously to predict Si and Mg isotope fractionation during evaporation [e.g., 2]. Earlier studies have also used chemical compositions and mineralogies of igneous CAIs to estimate pressures, temperatures and timescales of heating [5]. Yet there have been few if any systematic studies that relate *observed* isotope fractionations in CAIs to their conditions and timescales of formation.

In this study we apply what is known about the physical chemistry of CMAS melt evaporation and/or condensation to high-precision, *in-situ* LA-MC-ICPMS

$^{29}Si/^{28}Si$ data for CAI Levoille 144A, together with existing $^{25}Mg/^{24}Mg$ data for the object, to estimate the pressure (P_{H_2}) and time interval for its evaporation in the early solar nebula. We show that the time-P_{H_2} history of CAI 144A, and by analogy other similar igneous CAIs, can be reconstructed in detail by combining Si and Mg isotopic data for the object. The result is a unique univariant relationship between hydrogen pressure and time for melting of the CAI. This P_{H_2}-time constraint in turn limits the number of astrophysical settings for CAI melting and processing.

2. Analytical methods

We developed our laser-based silicon isotope ratio measurement technique using a multiple-collector double-focusing magnetic-sector inductively coupled plasma-source mass spectrometer (MC-ICPMS, ThermoFinnigan Neptune™). Three Faraday collectors were spaced to collect $^{28}Si^+$, $^{29}Si^+$, and $^{30}Si^+$ simultaneously. Potential molecular interferences for cardinal mass/charge (m/z) values corresponding to $^{28}Si^+$, $^{29}Si^+$, and $^{30}Si^+$ include $^{28}N_2^+$ and $^{12}C^{16}O^+$ for m/z=28, $^{14}N^{15}N^+$ and $^{12}C^{17}O^+$ for m/z=29, and $^{14}N^{16}O^+$ and $^{12}C^{18}O^+$ for m/z=30. The effects of these interferences were eliminated by operating with a mass resolving power (m/Δm) of ∼9000 (Fig. 1). Potential doubly-charged mass interference species and their first ionization potentials include $^{56}Fe^{2+}$ (m/z∼28, 16.18 eV), $^{58}Ni^{2+}$ (m/z∼29, 18.15 eV), $^{58}Fe^{2+}$ (m/z∼29, 16.18 eV), and $^{60}Ni^{2+}$ (m/z∼30, 18.15 eV). All of these doubly-ionized species have first ionization potentials substantially greater than that of Ar^+ (15.76 eV), with the result that none appears as a detectable species in the mass spectrum under our operating conditions. Corrections
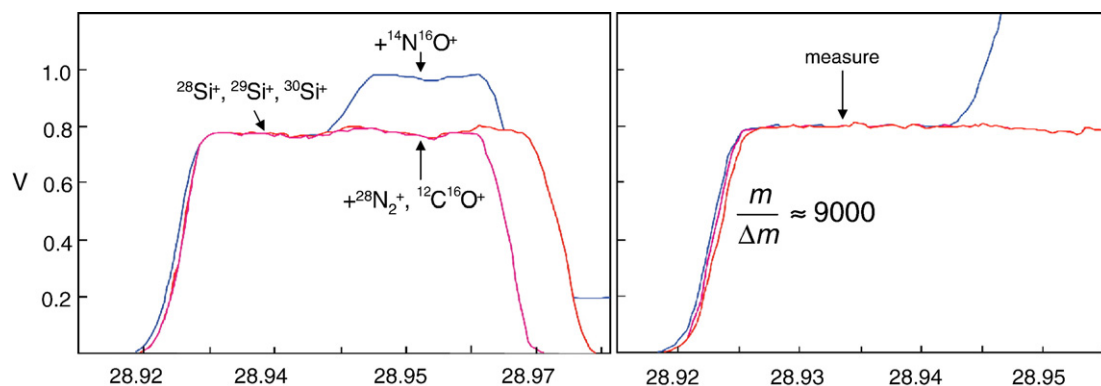

Fig. 1. Ion beam peak shapes for silicon obtained by LA-MC-ICPMS. The abscissa is approximate mass/charge based on the mass calibration on the day the data were taken. The ordinate is in voltage (10^{11} Ω amplifier resistors) but peaks are normalized to the maximum for easy comparison of shapes. Analyses were obtained on the peak flat on the low-mass side of interferences from N_2^+, NO^+, and CO^+. The mass resolving power m/Δm where m is the molecular/atomic mass (amu) is ∼9000.

for instrumental mass bias ($\sim 5\%$) were performed by sample-standard bracketing. Our in-house standard for this purpose is USNM #136718 forsterite (San Carlos olivine).

Isotope analyses were corrected by subtracting a preceding on-peak background measurement. Typical $^{29}Si^+$ signal intensities during CAI measurements were ~ 50 mV (using 10^{11} Ω amplifier resistors) and backgrounds for m/z=28, 29, and 30 were 4, 2, and 1 mV, respectively. Isotope ratio measurements during laser ablation consist of the mean of seven to ten ~ 4 s integration cycles. Sample and standard measurements were separated by a ~ 90 s interval.

All analyses are reported as per mil deviations from the standard such that

$$\delta^i Si = \left(\frac{(^i Si/^{28}Si)_{unknown}}{(^i Si/^{28}Si)_{std}} - 1 \right) \times 10^3 \qquad (1)$$

and where i refers to either 29 or 30. The usual international standard for Si isotope ratio measurements in natural samples is NBS-28 quartz [6,7]. Our working

standard, San Carlos olivine, has not been measured relative to NBS-28 (to the best of our knowledge) but is nonetheless a better standard for laser ablation because quartz does not couple as well with the laser beam. One can infer from previous studies of basalts, meteorites, and lunar rocks that San Carlos olivine $\delta^{29}Si$, representing Earth's mantle, could be $\sim -0.2\permil$ relative to NBS-28 [8,9]. Because our uncertainties are comparable to the likely difference between $\delta^{29}Si$ of San Carlos olivine and NBS-28, and because this difference between standards is also uncertain, we have not converted our $\delta^{28}Si$ values to the NBS-28 scale.

We used a 193 nm excimer laser operated with a pulse repetition rate of 2 to 6 Hz and UV fluence of between 21 and 27 J/cm^2. *In-situ* analyses were acquired from spots measuring 100 µm in diameter and ~ 20–30 µm deep. At this sampling scale melilite analyses, comprising the majority of the data, often include spinel in subordinate quantities (Fig. 2). The amount of spinel in each analysis varies from spot to spot. Ablation products of samples and standards were introduced to the mass spectrometer in a flow of He gas (0.5 l/min)
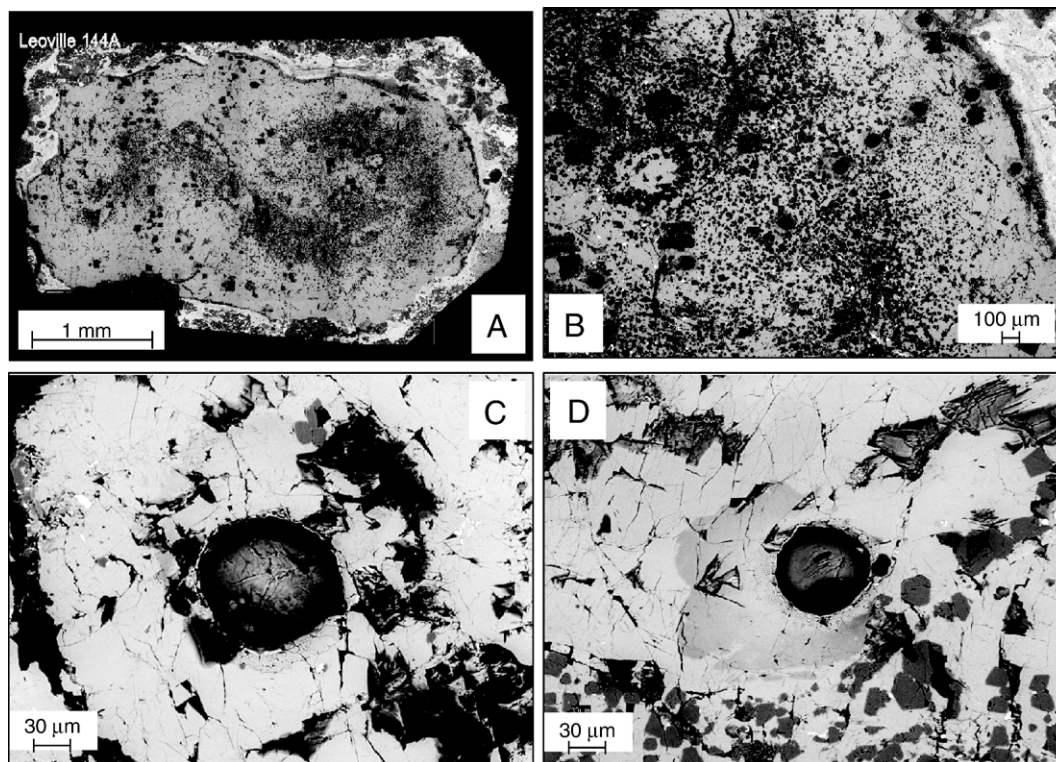

Fig. 2. Backscattered electron (BSE) images of CAI Leoville 144A. A: whole CAI embedded in surrounding matrix. Black spots are laser ablation pits from this Si isotope study and previous Mg and O isotope studies. B: melilite (medium grey) and spinel (dark grey) palisades (e.g., doughnut shape in left side of BSE image) in the northeast quadrant of the CAI. Black pits are various laser ablation craters. C: Close-up image of a laser ablation pit showing sparse inclusions of spinel in melilite. D: Close-up of laser ablation pit including melilite with no spinel visible at bottom of pit (cf. C). Slightly darker grey ring around laser pit is debris left from ablation.

[10]. Helium carried laser ablation products from the sample chamber to a mixing volume where it was combined with dry Ar gas (0.63 l/min). The sample + He + Ar mixture was then passed to the plasma source.

Precision of our LA-MC-ICPMS analyses is on the order of ±0.2‰ 1σ for both $\delta^{29}Si$ and $\delta^{30}Si$ based on replicate analyses of our standards. The accuracy of the Si isotope ratio results was assessed using a synthetic glass on the $CaMgSi_2O_6$–$CaAl_2Si_2O_8$ join ($Di_{0.59}An_{0.41}$) prepared with a 1% spike of ^{28}Si (Oak Ridge silicon batch no. 143292: 99.94% ^{28}Si; 0.04% ^{29}Si; 0.02% ^{30}Si). The gravimetric $\delta^{29}Si$ and $\delta^{30}Si$ values of the spiked glass based on the isotopic composition of NBS-28 (isotopically normal Si) [8] are −10.70 and −10.72‰, respectively. The glass was made from 1.083 mg of Oak Ridge ^{28}Si spike, 99.319 mg of NBS-28 SiO_2, 42.741 mg $Mg(OH)_2$, 89.359 mg $CaCO_3$ and 21.372 mg Al_2O_3. LA-MC-ICPMS analyses of this glass yield results indistinguishable from the gravimetric $^{29}Si/^{28}Si$ and $^{30}Si/^{28}Si$ values (Online Supplemental Material). Accurate analyses of the glass show that over the range of composition space spanned by our samples (e.g., from $Mg_{0.89}Fe_{0.11}SiO_4$ olivine to ∼$CaMg_{0.5}AlSi_2O_7$ glass), matrix effects are negligible. This result is consistent with previous studies using similar methods for Mg isotope ratio analysis by LA-MC-ICPMS [10–12].

3. Method for modeling CAI $^{29}Si/^{28}Si$ and $^{25}Mg/^{24}Mg$ variations

3.1. Model details

We modeled the isotopic evolution of CAIs, including rates of mass loss, time-dependent variations in isotope ratios, and time-dependent variations in elemental concentrations. The models consist of numerical solutions to the problem of elemental and isotopic fractionation at the moving surface of an evaporating sphere coupled with diffusional transport within the sphere. The shrinking sphere represents a volatilizing protoCAI where the rate of surface retreat is a function of the average volatility of the object as prescribed by differences between ambient and equilibrium vapor pressures of the constituent elements. The implicit finite difference scheme for solving this problem, akin to an inverse Stefan problem, was described previously [13]. We modified the implementation of the solution to the problem to account for the effect of Si and Mg isotope fractionation.

Isotope fractionation in a volatilizing CAI will have been controlled by the relative rates of evaporation and diffusion. Rates of CAI evaporation can be obtained from rates of its constituent Si, Mg, Ca, and Al. The total gas flux from a liquid CAI is given, to a good approximation [e.g., [2]], as $J_{total} \sim J_{SiO} + J_{Mg} + J_{Ca} + J_{Al} + J_{AlO} + J_{AlOH}$ where J_i is the molar evaporative flux of species i. Fluxes are calculated using a modified Hertz-Knudsen equation [3]:

$$J_i = \frac{\frac{\gamma_i(P_{i,eq} - P_i)}{\sqrt{2\pi m_i RT}}}{1 + \frac{\gamma_i r_o}{D_i^{gas}}\sqrt{\frac{RT}{2\pi m_i}}} \qquad (2)$$

where R is the gas constant, m_i is the mass of the species of interest (e.g., kg/mole), $P_{i,eq}$ is the equilibrium vapor pressure for the CMAS melt, P_i is ambient background vapor pressure of i, D_i^{gas} is the diffusion coefficient of i in the background gas (H_2), γ_i is the evaporation coefficient (dimensionless factor characterizing departures from the Hertz-Knudsen equation), and r_o is the original radius of the evaporating object. In practice, rather than calculating $P_{i,eq}$ explicitly, we used the parameterization of equilibrium vapor pressures given by equation 18 in Richter et al. [3]. The parameterization consists of a reference flux at a specific temperature and partial pressure of O_2 (a function of P_{H_2}) and an activation energy at fixed fugacity of O_2 of 650 kJ/mol [3]. Reference fluxes for SiO and Mg were taken from Table 1 of Richter et al. (experimental data for BCAI-SSI). Reference fluxes for Ca, Al, AlO, and AlOH were calculated from equilibrium vapor pressures for a CMAS melt given by Grossman et al. [2]. For all calculations shown here we used a value of 0.03 for γ_i in cases where γ is not already implicit in reference fluxes (see below) [3]. The use of a single, temperature-independent evaporation coefficient is consistent with incorporating the activation energy of 650 kJ/mol into the parameterization of fluxes [3].

Young and Galy [14] noted that Eq. (2) includes two distinct pressure effects on evaporation rate and isotope fractionation of a molten sphere in space. The first is the slowing of evaporation where P_i approaches $P_{i,eq}$ and the other is inefficient removal of evaporated gas species where total background pressure (∼P_{H_2}) inhibits diffusion in the gas phase. They noted that the presence of isotope fractionation in CAIs suggests that $P_i < P_{i,eq}$ and low P_{H_2} during CAI formation. Galy et al. [1] and Young and Galy [14] showed that since chondrules lack stable isotope fractionation, either P_{H_2} was higher than typical solar nebula values ($P_{H_2} > 10^{-3}$ bar) or P_i was elevated due to a high number density of chondrules during chondrule formation. Cuzzi and Alexander [15]

Table 1
Input for simulations of experimental studies [3,22] showing Si and Mg isotope ratio and chemical evolution of CMAS melts during evaporation

[a]Input	Si test, model 1	Mg test, model 2
T (K)	2073.15	1773.15
P_{H_2} (bar)	1.0×10^{-7}	1.87×10^{-4}
r (cm)	0.60	0.07
dr/dt (cm s^{-1})	7.2880×10^{-7}	1.5471×10^{-6}
J_{Mg} (mol cm^{-2} s^{-1})	1.8139×10^{-8}	4.1102×10^{-8}
J_{Si} (mol cm^{-2} s^{-1})	1.1887×10^{-8}	2.6952×10^{-8}
J_{Ca} (mol cm^{-2} s^{-1})	5.5472×10^{-12}	1.2599×10^{-11}
J_{Al} (mol cm^{-2} s^{-1})	1.5478×10^{-13}	3.5153×10^{-13}
J_{total} (mol cm^{-2} s^{-1})	3.0032×10^{-8}	6.8067×10^{-8}
$J_{Mg}/J_{Mg,congruent}$	3.3103	2.3182
$J_{Si}/J_{Si,congruent}$	1.0778	1.0913
$J_{Ca}/J_{Ca, congruent}$	6.0357×10^{-4}	7.1661×10^{-4}
$J_{Al}/J_{Al,congruent}$	1.7861×10^{-5}	2.1810×10^{-5}
$D^{28}Si$ (cm^2 s^{-1})	1.2000×10^{-5}	6.0000×10^{-7}
$D^{29}Si$ (cm^2 s^{-1})	1.198947×10^{-5}	5.994737×10^{-7}
$D^{24}Mg$ (cm^2 s^{-1})	2.4000×10^{-5}	1.2000×10^{-6}
$D^{25}Mg$ (cm^2 s^{-1})	2.390209×10^{-5}	1.195105×10^{-6}
DCa (cm^2 s^{-1})	2.4000×10^{-5}	1.2000×10^{-6}
DAl (cm^2 s^{-1})	1.2000×10^{-5}	6.0000×10^{-7}
$XMgO$	0.1825	0.2605
$XSiO_2$	0.3672	0.3628
$XCaO$	0.3060	0.2583
XAl_2O_3	0.1443	0.1184
V_{melt} (cm^3 mol^{-1})	24.2675	22.7288
$Pé^{28}Si$	0.03644	0.18050
$Pé^{24}Mg$	0.01822	0.09025
α 29/28	0.98980	0.98980
α 25/24	0.98689	0.98689

Model 1 simulates the experiments by Janney et al. [22]. Model 2 simulates the BCAI experiments of Richter et al. [3].

[a] Symbols: Xi = mole fraction of species i; V_{melt} = molar volume of melt, $\alpha i/j$ = isotope fractionation factor between species i and j. Others defined in text.

quantified the effect of chondrule number density on suppression of isotope fractionation and concluded that the number density of chondrules during their formation was at least 10 m^{-3}, corresponding to an average linear spacing between chondrules of 10 cm.

There is no *a priori* way of knowing $P_{i,eq} - P_i$ during CAI formation since fractionation ensures only that the inequality $P_{i,eq} > P_i$ obtains. Here we assume $P_{i,eq} >> P_i$ by setting P_i equal to zero in Eq. (2). The tacit assumption is that, unlike chondrules, the number density of CAIs during their formation was not sufficient to permit an overall elevation in background partial pressures of Mg and Si. We can quantify this assumption with an estimate of the pressure of gas molecules or atoms i produced by a population of evaporating CAIs. Results (see Online Supplemental Material) for melting time spans of 6 to 48 h (representing probable timescales for individual melting

events constrained by cooling timescales [16]) show that $P_i/P_{i,eq}$ becomes significant for CAI number densities of 10^{-3} m^{-3} to 2 m^{-3}, or an average linear spacing between CAIs of ~ 8 to 0.8 m. Since the transition between effective vacuum ($P_i/P_{i,eq} \sim 0$) and equilibration ($P_i/P_{i,eq} = 1$) is abrupt in comparison to all possible number densities, we conclude that CAIs are fractionated because their linear spacing was more than ~ 8 m during their formation. The alternative of allowing for a reduced evaporation rate due to a finite $P_i/P_{i,eq}$ value between 0 and 1 requires a just-so spacing between CAIs of between 8 and 0.8 m (we cannot, however, reject the possibility that there was another source of Mg and Si in the region of CAI formation). Note that our calculated maximum number density of CAIs is 4 orders of magnitude lower than that calculated for chondrules [15]. In any event, by assuming $P_i/P_{i,eq} = 0$ in our calculations we are invoking a linear spacing of >8 m for CAIs in the vicinity of 144A.

The r.h.s. denominator term in Eq. (2) corrects for return of evaporated species due to a finite diffusion through the surrounding gas at higher pressures. The denominator in Eq. (2) also relates the isotope fractionation factor associated with evaporation to that where return flow is important. This relationship is given by Richter et al. [3] and was built into our model calculations. In practice the pressure threshold where the denominator in Eq. (2) deviates noticeably from 1 (i.e., $P_{H_2} > 10^{-3}$ bar) is greater than most plausible solar nebula environments.

Total gas flux can be combined with the molar volume of the CMAS melt, $\hat{V}_{melt}$, obtained from CMAS partial molar volumes [e.g., 17], to arrive at the rate of evaporation expressed as a shrink rate of the molten sphere:

$$dr/dt = \dot{r} = \hat{V}_{melt} J_{total}. \tag{3}$$

This evaporative shrink rate, the pre-evaporative radius of the object r_o, and the diffusivity of the element of interest in the condensed phase, D_i, together determine the Péclet number for species i, or $Pé_i$, such that

$$Pé_i = -r_0 \frac{\dot{r}}{D_i} \tag{4}$$

and the negative sign accounts for a negative dr/dt (shrinking sphere). The value for $Pé_i$ specifies the importance of advective transport (surface retreat due to evaporation) relative to diffusive transport of i (diffusion in the condensed phase) and can be used to predict not only the bulk isotopic composition of the residual

evaporating liquid or solid but also the degree of isotope zoning caused by evaporation in the condensed phase [13]. Where $Pé_i \geq 0.1$, substantial zoning in chemical and isotopic concentrations are to be expected. The parameterization of evaporation fluxes provided by Richter et al. [3] and Grossman et al. [2], CMAS partial molar volumes of Courtial and Dingwell [17], and diffusion coefficients for Si, Mg, Ca and Al in silicate melts [18,19] permit one to calculate the temperature and P_{H_2} conditions under which CAI melts acquired their Si and Mg isotope ratios.

With the above thermochemical and kinetic data, the distribution of light element isotopes in CAIs can be calculated using the method described by Young et al. [13]. Calculated bulk isotope ratios and isotope ratio zoning patterns are obtained by solving the equation

$$\frac{\partial c_{i,\text{cond}}}{\partial t} = D_i \left(\frac{\partial^2 c_{i,\text{cond}}}{\partial r^2} + \frac{2}{r} \frac{\partial c_{i,\text{cond}}}{\partial r} \right) \qquad (5)$$

where $c_{i,\text{cond}}$ is the concentration of species i in the condensed phase and r is the radial position within the object. Eq. (5) can be solved subject to the boundary conditions $\partial c_{i,\text{cond}}/\partial t = 0$ at $r = 0$ and

$$D_i \frac{\partial c_{i,\text{cond}}}{\partial r} \Big|_{r=s(t)} = c_{i,\text{cond}}(J_i/J_{i,\text{cong}} - 1) \ \dot{r} \qquad (6)$$

at the moving surface $r = s(t)$ of the evaporating object. In Eq. (6) $J_{i,\text{cong}} = x_i \dot{r}/\hat{V}_{\text{melt}}$ is the molar congruent flux for i where x_i is the mole fraction of i in the condensed phase. Congruent flux refers to the evaporative flux of the species in the absence of species-specific vapor pressures. In the dimensionless form of Eq. (5), $Pé_i$ is the negative of the rate of surface migration due to loss of species i [13]. We emphasize that Eqs. (5) and (6), originally derived by Young et al. [13] for congruent evaporation, are appropriate for incongruent evaporation when the fractionation factor α is replaced by the flux ratio $J_i/J_{i,\text{cong}}$ in Eq. (6) [20]. The latter flux ratio is the effective elemental partitioning due to volatility for each isotopologue species. For such a calculation each isotopic species has a distinct diffusivity D_i and Peclet number $Pé_i$. The formulation of the problem given by Richter et al. [3] is virtually identical to that described here; these workers replaced the $Pé_i$ used by Young et al. [13,20] with "evaporation numbers", E_{vi}. It is straightforward to show that $Pé_i = E_{vi}/3$.

Solutions for concentrations of elements using Eqs. (5) and (6) are obtained by solving the equations numerically (implicit finite difference) for each element relative to the others (i.e., pseudo-binary calculations) and renormalizing the resulting concentrations for each

element to the total. Isotope ratios are obtained by solving for each isotopologue separately and then taking the ratio of the results. Evaporation isotope fractionation factors α define the isotope specificity of evaporation at the surface of the condensed phase because $\alpha = J'_i/J_i$ where ' signifies the rare isotopologue. When evaluating the equations one takes into account the small differences in diffusivities between the isotopes as well as the different evaporative fluxes [21]. Here, we use the expression $D'_i/D_i = (m_i/m'_i)^\beta$ where m_i is the mass of the diffusing species. For Si we use a β of 0.025 based on experimental measurements of Ge diffusion [21] and for Mg we use a β of 0.10 based on analogy with diffusion of Ca [21]. The β values for Ca and Al were both taken to be 0.10. In all cases these values for β are small compared with the purely theoretical value of 0.5 but they nonetheless play an important role in controlling isotope fractionation in the interior of the evaporating object where $Pé_i > 0.1$.

3.2. Validation

In order to validate our calculation scheme we modeled the measured changes in Mg isotope ratios and chemical compositions attending evaporation of type B CAI-like liquids in the laboratory ("BCAI" experiments) reported by Richter et al. [3] and Si isotope fractionation measured for analogous experiments reported by Janney et al. [22]. These models of experiments test our ability to capture the physical chemistry of incongruent evaporation with our calculations. Inputs for the models are listed in Table 1. We performed our calculations at $T = 2073$ K and $P_{H_2} = 1 \times 10^{-7}$ bar for the Si calculations (model 1) and at $T = 1773$ K and $P_{H_2} = 1.87 \times 10^{-4}$ bar for the Mg calculations (model 2), matching the conditions of the respective experiments.

Chemical diffusion is more rapid than tracer diffusion of major elements in these melts and evaporation can lead to chemical gradients as well as isotopic gradients. Accordingly, we used the chemical diffusivities for Mg, Si, Ca, and Al in CMAS melts indicated by Kress and Ghiorso [19], Liang et al. [18], and references therein. Rates of diffusion in the melt phase depend on the direction in composition space followed, but in general a review of the diagonalized diffusion matrices for melts in the systems CAS and CMAS suggests that at 1773 K $D_{Mg} \sim 1.2 \times 10^{-6}$ cm^2 s$^{-1} \sim D_{Ca} \sim 2 \times D_{Si} \sim D_{Al}$. Some of the melts used to derive these diffusivities have SiO$_2$ concentrations greater than CAIs. Relationships between viscosity, silica content, and diffusivity imply that we could be underestimating D_i by as much as a factor of 5 (based on

experimental C(M)AS SiO_2 concentrations of 50% vs. 25% for CAIs) with the effect that $Pé_i$ may be overestimated by as much as 5×. Typical activation energies (E_a) for diffusion in relevant systems suggest a median E_a of 300 kJ/mol. This value was used to account for temperature (Table 1).

Our evaporation rates (i.e., shrink rates) match those of the experiments, as they must, because our reference fluxes were derived from these experiments. What is more, we find that the evaporation rates derived from the parameterized thermodynamics [3] also successfully predict the measured evaporation rates of forsterite (solid or liquid) [23]. For example, Naghahara and Ozawa [23] measured evaporation fluxes for solid forsterite in 2×10^{-7} bar of H_2 gas at 1973 K of 6.9×10^{-7} to 1.1×10^{-6} g cm^{-2} s^{-1}. The calculated value using the parameterized thermodynamics is 1.0×10^{-6}. Similarly, at 6×10^{-4} bar H_2 Nagahara and Ozawa obtained a flux of 5.4×10^{-5} g cm^{-2} s^{-1} that compares well with the calculated value of 5.8×10^{-5}. Although the parameterization of the thermodynamics was derived from type B CAI melt compositions, the ability to successfully predict forsterite evaporation rates shows that the calculations are valid over a range of compositions, encompassing at the least the compositional joins from CMAS to Mg_2SiO_4.

We calculated the evaporation histories of ^{28}Si, ^{29}Si, ^{24}Mg, ^{25}Mg, Ca, and Al under the appropriate experimental conditions [3,22] using the "BCAI" starting composition. The calculations simulate the chemical and Si and Mg isotopic compositions of the residual melts in the experiments. Our results were compared with the bulk Si and Mg isotope ratios and bulk chemical compositions of evaporative residues reported by Janney et al. and Richter et al. Bulk compositions in our models are obtained by integrating each chemical parameter with respect to the radius of the model spherical residue.

The calculations show that our models accurately reproduce the experimental results for both Si and Mg isotope fractionation using the fractionation factors of 0.9898 and 0.9869, respectively (inset Fig. 3). These fractionation factors are the same as those reported in the original studies and verify that diffusion played a negligible role in determining the bulk isotopic compositions of the experimental products. Our calculations also faithfully reproduce the chemical evolution of the bulk products with up to 70 to 80% mass loss of Mg (% mass loss refers to $100(1 - Mg/Mg_o)$ or in general $100(1 - F_i)$ where F_i is the fraction of element i remaining) (Fig. 3). Beyond $\sim 80\%$ mass loss the accuracy of the assumption of a constant rate of evaporation begins to break down as the bulk composition becomes substantially more refractory than the initial composition (approaching pure Ca and Al). The model calculations used in the present study are within the range of compositions where $\dot{r}$ can be assumed to be constant. Our calculations also faithfully reproduce the
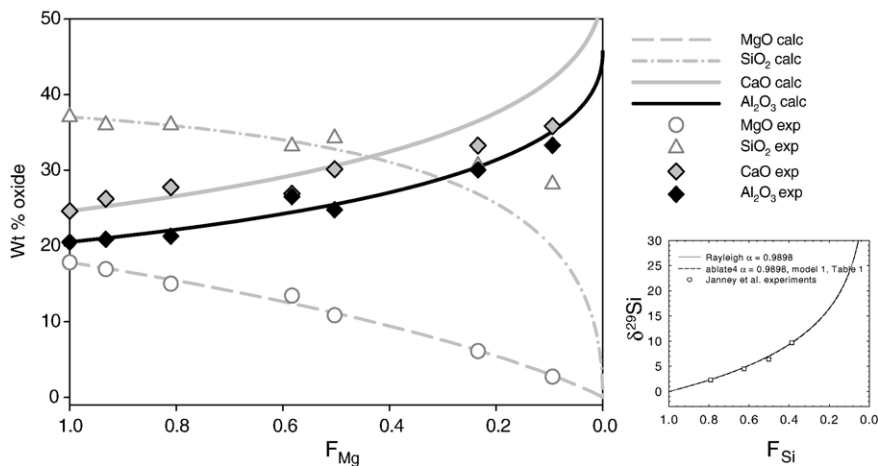

Fig. 3. Calculated changes in weight per cent MgO, SiO_2, CaO, and Al_2O_3 (using ablate4) as a function of Mg remaining (F_{Mg}) as a consequence of evaporation compared with published experimental data for these oxides in evaporative residues of quenched CAI melts. The experimental data are from the BCAI runs reported by Richter et al. [3]. The calculated evolution curves represent model 2 in Table 1. The calculated evolution curves fit the data satisfactorily with a constant dr/dt with up to $\sim 80\%$ Mg loss, beyond which the assumption of a constant evaporation rate breaks down as CaO and Al_2O_3 dominate the residue. The inset shows the experimentally-derived data for $\delta^{29}Si$ vs. F_{Si} (fraction of Si remaining) reported by Janney et al. [22] for $T = 2073$ K and $PH_2 = 10^{-7}$ bar compared to the model for evaporation at the same conditions obtained with the code used in this study (ablate4.f, dashed curve) and pure Rayleigh fractionation with the same fractionation factor (solid curve).

Table 2
Laser ablation MC-ICPMS Si isotope ratio analyses of CAI Leoville 144A

Laser spot	Distance [a] (μm)	$\delta^{29}Si_{SC}$ [b]	1σ [c]	$\delta^{30}Si_{SC}$	1σ
1	780	3.12	0.11	5.56	0.11
2	530	3.62	0.17	6.43	0.12
3	1600	3.19	0.19	6.23	0.16
4	970	3.55	0.17	6.76	0.12
5	200	3.36	0.19	5.93	0.16
6	70	4.26	0.09	7.90	0.12
7	1400	3.36	0.13	5.84	0.10
8	120	3.71	0.11	7.53	0.12
9	100	4.01	0.16	7.69	0.10
10	350	3.01	0.20	5.92	0.15
11	1100	3.26	0.12	6.77	0.12
12	600	3.54	0.14	7.05	0.11
13	420	3.45	0.09	6.80	0.08
14	1180	3.55	0.17	6.56	0.12
15	90	4.58	0.08	8.46	0.12

[a] Distance from outer edge of CAI.
[b] δ values are per mil deviations from San Carlos olivine.
[c] Internal precision represents standard error for measurement cycles comprising each analysis.

experimental timescales of evaporation (e.g., 180 min for 40% loss of Mg, not shown), verifying the applicability of Eq. (3).

4. Sample description

Leoville 144A is a 10×6 mm compact type A inclusion from a section of the Natural History Museum (NHM) #144 sample of the CV3 meteorite Leoville (Fig. 2A). It is composed mainly of melilite (Ak_{10-25}), magnesian spinel, minor Al–Ti-rich diopside with ~ 10 wt.% Ti_2O_3 and 7 wt.% TiO_2, and minor perovskite typically associated with diopside. The CAI is mantled by a Wark-Lovering rim composed of hibonite laths, spinel, and perovskite as well as relatively Ti-poor diopside. The object has been studied extensively [11,24]. It has typical igneous CAI oxygen isotope systematics with $\delta^{18}O \sim \delta^{17}O$ ranging from -40‰ to 0‰ relative to standard mean ocean water (SMOW) [25] and with most, but not all, values spread along the carbonaceous chondrite anhydrous mineral (CCAM) mixing line in oxygen three-isotope space. Magnesium isotope ratios define radiogenic excesses in $^{26}Mg/^{24}Mg$, $\delta^{26}Mg^*$, corresponding to an initial $^{26}Al/^{27}Al$ of 6×10^{-5} [11]. The oxidation state of Ti in the interior of the object suggests that it crystallized with a fugacity of oxygen (f_{O2}) defined by a gas of $\sim$ solar composition [24]. In brief, Leoville 144A is an unremarkable, typical,

albeit rather large, igneous type A CAI from a CV3 meteorite.

5. Isotope ratio results

Silicon isotope ratios for CAI Leoville 144A are listed in Table 2. The fifteen LA-MC-ICPMS analyses of $^{29}Si/^{28}Si$ and $^{30}Si/^{28}Si$ in 144A show no signs of anomalous (i.e., mass-independent) Si isotope fractionation (Fig. 4). For this reason we can confine our discussion to $\delta^{29}Si$ values only.

The $\delta^{29}Si$ values are essentially uniform across the object with an average of 3.6 ± 0.4‰ 1σ. There is a detectable increase in $\delta^{29}Si$ at the margin of the object of about 1‰ relative to the interior (Fig. 5). Excluding the two points within 100 μm of the edge of the inclusion gives an average $\delta^{29}Si$ of 3.4 ± 0.3‰.

The $\delta^{29}Si$ values of 144A are approximately half those of its $\delta^{25}Mg$ values (Fig. 5). This relationship of $\delta^{29}Si \sim 1/2\ \delta^{25}Mg$ is similar to that seen in previously published bulk CAI isotope data [4] and is the result of the relative mass differences between the isotopes of each element and the relative concentrations of SiO_2 and MgO (see below). High $\delta^{29}Si$ values at the margin of the inclusion are consistent with high $\delta^{25}Mg$ at the margins as well [24] (Fig. 5).

6. Comparisons with models

Model calculations can be used to constrain the history of CAI 144A (and by inference, other similar CAIs) using the new Si data presented here and the previously published Mg isotope ratios for the object. In
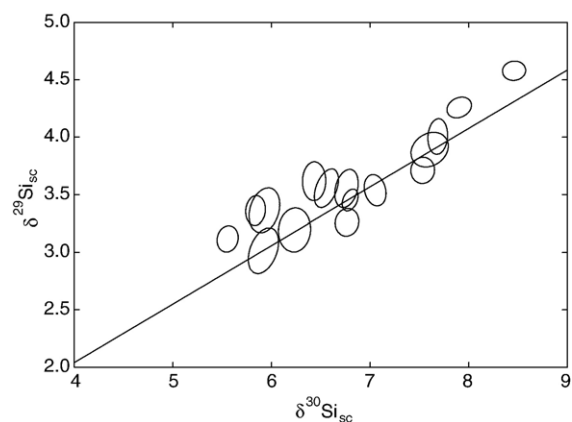

Fig. 4. Silicon three-isotope plot showing the terrestrial mass fractionation line and data for CAI Leoville 144A. The data are shown as 1σ error ellipses for each datum. Delta values are per mil deviations from the San Carlos olivine standard.
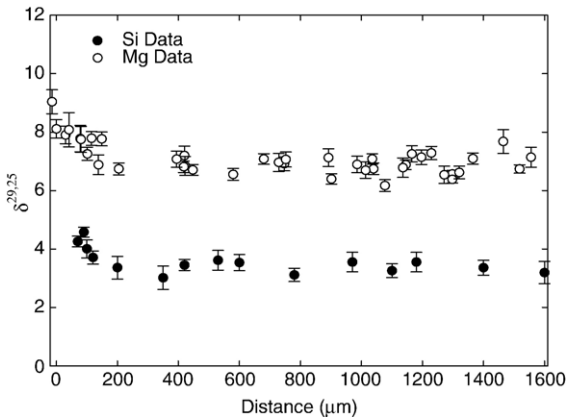
Fig. 5. Comparison of radial δ^{29}Si (closed symbols, this study) and δ^{25}Mg (open symbols [24]) profiles for CAI Leoville 144A relative to San Carlos olivine. Ordinate is the distance of the center of each laser ablation spot from the edge of the CAI. Note the increase in both Si and Mg stable isotope fractionation at the margin of the object. Error bars are 1σ.

particular, we wish to know the cause of the high δ^{29}Si and δ^{25}Mg in this igneous CAI. We also wish to learn what processes controlled the shape of the zoning pattern from core to rim. Critical observations to be explained/reproduced are the relationship δ^{29}Si ~ 1/2 δ^{25}Mg, the uniform δ^{29}Si and δ^{25}Mg values across most of the CAI, and the high δ values at the margin (excluding the Wark-Lovering rim where δ^{25}Mg is ~ chondritic or lower [24]).

In lieu of experiments on compact type A compositions we use the experiments on type B CAIs (usually containing greater MgO than compact type As [2]) as a guide to temperatures for the melt. Experiments on type B CAIs [26] suggest solidus temperatures near 1650 K and liquidus temperatures of ~1850 K. We therefore present our calculations for evaporating CMAS melt at three representative temperatures: 1673 K (~spinel+ melilite+liquid), 1773 K (~spinel+liquid), and 1873 K (liquid). For convenience, we refer to the 1773 K calculation when describing the results of the models unless otherwise specified.

6.1. Bulk δ^{29}Si and δ^{25}Mg

The bulk δ^{29}Si and δ^{25}Mg values constrain the thermal history of CAI 144A. By determining the time at which both silicon and magnesium bulk delta values reached the measured values, we obtain a univariant relationship between time and P_{H_2}. We emphasize that a unique relationship between time and pressure would not be constrained with δ^{25}Mg or δ^{29}Si alone, and that it is the combination of the two isotope ratios that yields

the sought after result. We also point out that the combination of the two isotope systems permits us to solve for the initial concentrations of Si and Mg in the object prior to its evaporation.

We calculated δ^{25}Mg and δ^{29}Si as a function of hydrogen pressure from 10^{-4} to 10^{-9} bar. This pressure range represents conditions ranging from maximum pressure estimates for the solar nebula to a hard vacuum. At $P_{H_2} > 10^{-4}$ bar the timescales we derive are similar to those at 10^{-4} bar and at $P_{H_2} < 10^{-9}$ bar timescales change little from those at 10^{-9}, obviating the need to consider P_{H_2} values beyond the chosen range. Where calculations match the measured δ^{25}Mg and δ^{29}Si, the evaporation timescale, initial concentrations, and final concentrations are determined as functions of P_{H_2}. The result illustrates that as P_{H_2} increases the fluxes of the evaporating species, and therefore the time required to reach the observed fractionations, decreases (Fig. 6). The loci of pressure-dependent crossing points can be used to produce isotherms showing the time vs. P_{H_2} relationship required by the measured Si and Mg isotope ratios over the range of plausible temperatures (Fig. 7). These isotherms in log(t) vs. log(P_{H_2}) space are linear from $P_{H_2} \sim 10^{-4}$ to 10^{-8} as required by the dependence of J_i on $\sqrt{P_{H_2}}$ [3]. At $P_{H_2} > 10^{-4}$, diffusion in the melt becomes limiting and the curves begin to merge. At $P_{H_2} < 10^{-8}$ bar evaporation timescales become independent of pressure.

The resulting univariancies in Fig. 7 reveal the time required to reach the observed fractionations among Si and Mg isotopes as a function of P_{H_2}. This result does not imply necessarily that the CAI was molten
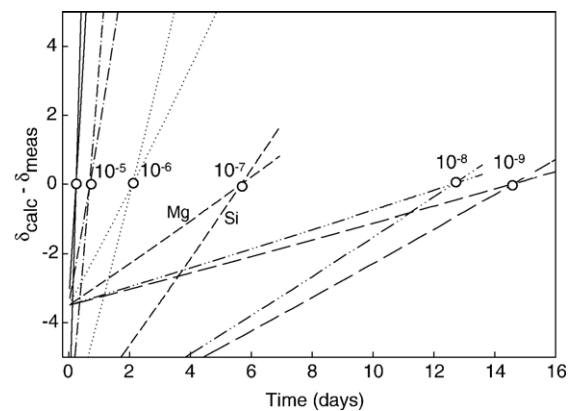

Fig. 6. Array of calculated points in time-δ^{29}Si and δ^{25}Mg space where both δ^{29}Si and δ^{25}Mg match the observed values in CAI Leoville 144A. Each crossing point shows where both Si (steeper lines) and Mg (shallower lines) isotope data for 144A are matched by calculations at the indicated P_{H_2}. The plot shows how time of evaporation constrained by the isotope data relates to P_{H_2}.
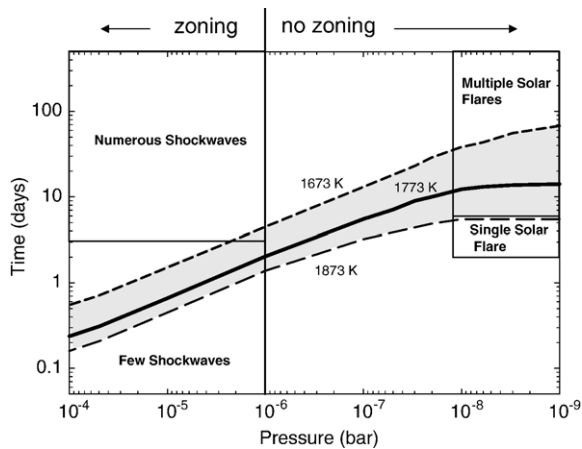
Fig. 7. Calculated P_{H_2}-time curves for evaporation of a molten CAI like Leoville 144A at 1673 K (near solidus), 1773 K, and 1873 (near liquidus) K. The curve represents the loci of points shown in Fig. 6, with each point corresponding to the conditions under which both $\delta^{29}Si$ and $\delta^{25}Mg$ match the observed values. Also shown are regions in P_{H_2}-time space corresponding to melting by encounter with a small number (e.g.,<5) of gas shock fronts, a large number of shock fronts, a single solar flare in the inner annulus of the protoplanetary disk, and multiple solar flares. The derivation of the region in P_{H_2}-time space occupied by each astrophysical setting is described in the text. The figure shows that encounters with either a relatively few number of shock fronts or many solar flares (e.g., of order 10) can explain the melting and volatilization of Leoville 144A. Exposure to a single flare and a large number (e.g., >5) of shock fronts are excluded as possible causes of melting.

continuously over the indicated time spans. Rather, they indicate the cumulative times in the liquid state required by the isotope data. For example, 15 days in the molten state (i.e., the maximum for the 1773 K isotherm) might well represent 15 individual 1-day melting events. Fig. 7 depicts the unique solution for 144A, but the same principle can be applied to other igneous CAIs. Results for other CAIs will yield curves similar in shape to those in Fig. 7 but displaced vertically at low pressures depending upon the degree of isotope fractionation. All such curves for different CAIs must converge to short timescales at high pressures (hours at $P_{H_2} \le 10^{-4}$ bar) but will exhibit more variation in duration of melting at lower pressures in accordance with their different isotopic fractionations.

It is clear from Fig. 7 that CAI 144A was molten for a cumulative time of no more than 70 days. If evaporation occurred ~100° above the solidus, the timescale was less than 15 days.

The calculations also show that the precursor to the melted 144A object was already CAI-like in composition. In order to satisfy the observed isotope ratios at all temperatures and pressures investigated, the CAI had to

have had specific and well-defined initial concentrations of SiO_2 and MgO of 23±2 wt.% and 15±2 wt.%, respectively, with the remainder plausibly evenly split between CaO and Al_2O_3, e.g., 31% CaO, and 31% Al_2O_3 (the final result is not sensitive to the relative proportions of CaO and Al_2O_3). This starting composition is more calcic and aluminous than typical chondrite and points to a CAI-like precursor to the melted object not unlike that predicted from the condensation trends for CAI precursors calculated by Grossman et al. [2]. The final compositions of the evaporated residues in the models are all essentially the same at $P_{H_2} < 1 \times 10^{-4}$ bar. The final composition is 10.05±0.05 wt.% MgO, 18.80±0.2 wt.% SiO_2, 35.6± 0.1 wt.% CaO, and 35.6±0.1 wt.% Al_2O_3. The uncertainties here represent the range of final compositions constrained by the models at $P_{H_2} = 10^{-9}$ to 10^{-4} bar and are likely to be numerical in origin. At 10^{-4} bar the final composition is slightly different with 9.9 wt.% MgO, 16.6 wt.% SiO_2, and again the remainder equally divided between CaO and Al_2O_3. We do not have a whole-rock chemical analysis of 144A (much of the object not in thin section was dissolved for bulk Mg isotope work) but the model final compositions we derive are consistent with typical igneous CAI bulk composition [2].

6.2. $\delta^{29}Si$ and $\delta^{25}Mg$ radial profiles

The time intervals for CAI melting determined from the whole-rock calculations can be used to calculate the expected variations in $\delta^{29}Si$ and $\delta^{25}Mg$ as a function of radius across the CAI. At pressures $<10^{-6}$ bar the calculated profiles are relatively flat for both $^{29}Si/^{28}Si$ and $^{26}Mg/^{24}Mg$ (Fig. 8). This is because the Péclet numbers associated with these models are sufficiently low that diffusion is not a limitation to the evaporative flux (Fig. 8). At $P > 10^{-6}$ bar detectable isotope ratio zoning is expected (Fig. 8). The Péclet numbers at these higher pressures are >0.1.

The relatively flat calculated isotope ratio profiles at $P_{H_2} < 10^{-6}$ bar match the data for the interior of the CAI (the sharp increases in $\delta^{29}Si$ and $\delta^{25}Mg$ do not match any of the profiles calculated for the liquid state, see below). In the simplest interpretation, the lack of zoning (except near the margin) suggests that the CAI melted at $P_{H_2} < 10^{-6}$ bar. Such a low pressure would place an important constraint on the astrophysical environment for CAI melting.

It is possible, however, to circumvent the conclusion that the CAI was melted at $P_{H_2} < 10^{-6}$ if annealing in the solid state is invoked. In this scenario, the isotope ratio

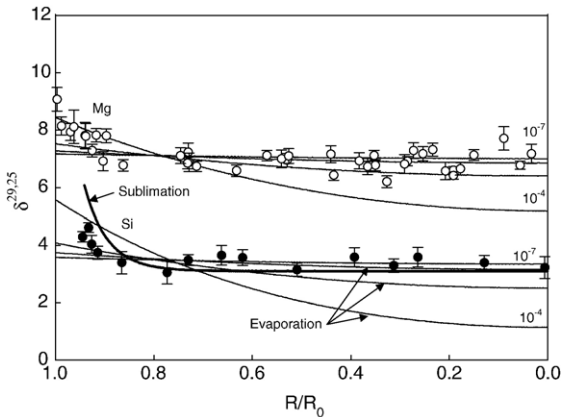Fig. 8. Plot of δ^{29}Si (closed symbols, this study) and δ^{25}Mg (open symbols [24]) versus distance from the center of CAI Leoville 144A (distance is normalized to the maximum radial distance R_o) compared with calculated variations in δ^{29}Si and δ^{25}Mg with radial position in the CAI. Thin model curves represent evaporation models where the bulk δ^{29}Si and δ^{25}Mg values match those of CAI Leoville 144A. Evaporation curves are shown for P_{H_2} of 10^{-7}, 10^{-6}, 10^{-5}, and 10^{-4} bar (10^{-9} and 10^{-8} bar contours are indistinguishable from the 10^{-7} contour) at 1773 K. These pressures correspond to ^{28}Si Péclet numbers of 0.03, 0.08, 0.21, and 0.67, respectively and ^{24}Mg Péclet numbers of 0.013, 0.03, 0.09, and 0.28, respectively. The plot shows that measurable Si and Mg isotope ratio zoning should be present in the CAI if P_{H_2} during melting was $\geq 10^{-6}$ bar (or $Pé_i \geq 0.1$). Also shown in bold is the curve representing sublimation of the solid CAI for 10 yr at $T = 1300$ K and $P_{H_2} = 10^{-7}$ bar. Sublimation like that modeled here is required to explain the sharp gradients in δ^{29}Si and δ^{25}Mg in this object. Misfit between the calculated sublimation curve and the data is discussed in the text.

zoning incurred at higher pressures is eliminated by diffusive isotopic redistribution at high temperatures in the solid state (where evaporation is limited by diffusion to a relatively narrow boundary layer). It is straightforward to obtain an estimate of the time required to relax a silicon or magnesium isotope ratio gradient in a solid CAI. For example, starting with a gradient in δ^{29}Si and a target of homogenization of δ^{29}Si values to within 10% of the bulk δ^{29}Si value (in our case implying homogeneity at the 0.3‰ level), the time scale for isotopic equilibration is given, to first order, by the expression

$$0.1 = \exp(-\pi^2 (D_i t/r)) \qquad (7)$$

where D_i is the solid-state diffusion coefficient of the element of interest, t is the time elapsed, and r is the radius of the object [27]. For a radius of 0.3 cm (matching 144A), a subsolidus temperature of 1300 K, and a tracer diffusion coefficient for Si in melilite of $\sim 3 \times 10^{-12}$ cm²/s [28], we find that an isotopically zoned object like 144A would have homogenized in

500 yr. This calculation relaxes the pressure constraint imposed by the bulk Si and Mg isotope ratios of the object *but does not* compromise the applicability of the univariancy in P_{H_2}-time space shown in Fig. 7. However, if this annealing occurred at $P_i < P_{i,eq}$, evaporation would have resulted. The initial evaporation rate for a solid CAI like 144A at 1300 K, based on Eq. (3), is 7×10^{-11} cm s^{-1}, suggesting that there would have been substantial mass loss in 500 yr (e.g., $\dot{r}$(cm/yr)/ 500 yr suggests a lifetime of 140 yr). However, the high $Pé_i$ values associated with solid evaporation would confine Al and Ca enrichment to the margins of the object and $\dot{r}$ would have decreased once the margin lost >70% of its Si and Mg. Also, it has been suggested that annealing of CAIs could have occurred at higher P_{Mg} and P_{Si}, minimizing subsolidus evaporation [24]. Exposure to high subsolidus temperatures for hundreds of years is consistent with the time-scale and temperatures necessary to reset the ^{26}Al–^{26}Mg clock in many CAIs [11]. Complete resetting of the ^{26}Al–^{26}Mg clock, resulting in a canonical or near canonical initial ^{26}Al/^{27}Al value, did not occur in 144A since it has supracanonical ^{26}Al/^{27}Al, though some perturbation of the radiogenic system is evident [11].

In order to explain the formation of the upturn in δ^{29}Si and δ^{25}Mg towards the rim of 144A, a late-stage heating and evaporation event in the solid state must be invoked. We modeled this final event using the tracer diffusivity of Si, a radius of 0.3 cm to match the size of 144A, and an evaporation rate defined by the thermodynamic models used in the liquid models. The latter is justified by the well-known continuity of evaporation rates across the liquid–solid phase transition and is born out by evaporation data for solid and molten forsterite [23,29]. We assumed P_{H_2} was sufficiently low (10^{-7} bar) that back reaction was unimportant and evaporation rate was moderate. The rate of evaporation, size, and diffusivity combine to give a $Pé_{Si}$ of 53.4 in this calculation. The value for $J_{Si}/J_{Si,cong}$ is 1.293. We use a ^{29}Si/^{28}Si fractionation factor at the surface of the evaporating sphere of 0.9898. Results (Fig. 8, bold solid curve) show that the upturn in δ^{29}Si at the margin of 144A is consistent with evaporation of the CAI as a solid for a cumulative timescale of ~ 10 yr at high temperatures (~ 1300 K). Similar results are obtained for δ^{25}Mg. Higher pressures would shorten this timescale up to 10^{-3} bar, beyond which fractionation would be hindered by return of the lighter isotopes to the solid surface. Lower temperatures would lengthen the required timescale for annealing. In this run the CAI was reduced in size by half, but the calculation is inaccurate because, once again, the rate of evaporation would have slowed

once Mg and Si were depleted by more than $\sim 70\%$, something not accounted for when using a fixed $\dot{r}$. This lack of a time-dependent $\dot{r}$ most likely plays a role in precluding a perfect fit to the data at the margin since $Pé_{Si}$ will also have evolved to lower values (Fig. 8).

The combination of Si and Mg isotope ratios in CAI 144A point to a thermobarometric history involving a period of supersolidus evaporation for ~ 1 to 70 days followed by late-stage sublimation lasting years. If lack of isotope ratio zoning resulted from reequilibration by tracer diffusion in the solid state, then a post-melting interval of heating lasting $\geq 10^2$ yr is implied. We emphasize that the times referred to here are integrated and may represent the cumulative effects of numerous shorter events.

7. Astrophysical implications

The Si and Mg isotope data for 144A place important constraints on where in the solar protoplanetary disk the CAI may have been melted and subsequently heated. Among existing models for processing solids in the early solar system, there are at least two plausible astrophysical settings for the melting of this igneous CAI and, by extrapolation, other igneous CAIs with similar isotope systematics. One is melting by passage of the CAI into shockwaves resulting in an integrated melting interval of hours to one or two days and the other is exposure to many solar flare events in the early solar system amounting to a total melting time of no more than ~ 70 days (Fig. 7). This excludes many other possibilities. For example, hundreds of melting events by shock heating or melting by a single solar flare are excluded by the mass fractionation exhibited by the CAI (Fig. 7), as shown below.

The shockwave model for heating chondrules and igneous CAIs predicts that millimeter sized objects passing through a high-density gas front at supersonic velocities experience temperatures of 1400 K to 2200 K for roughly one day with radiative heating above ambient temperatures for several days. Time scales for melting are expected to be on the order of hours. Pressures in the shock exceed ambient by a factor of 10 to 100 [30]. Assuming the solar protoplanetary disk mass was in the range from 0.02 $M_{\odot}$ (the minimum) to 0.13 $M_{\odot}$ (a reasonable large value), the calculations by Boss et al. [31] suggest a range in ambient midplane pressures in the inner disk ($R < 5$ AU) from 10^{-7} bar ($R = 5$ AU, 0.02 $M_{\odot}$, gas number density $= 4 \times 10^{11}$ cm^{-3}) to 10^{-4} bar ($R = 1$ AU, 0.13 $M_{\odot}$, gas number density $= 4 \times 10^{14}$ cm^{-3}). Therefore, if melting of 144A occurred in a shockwave, the likely pressure was between 10^{-6} bar to 10^{-3} bar for a time span of the order of a day or less. These conditions are consistent with the high-pressure end of the univariant time-pressure trajectory for 144A required by its Si and Mg isotope ratios (Fig. 7). Shockwave heating would imply that the CAI was at one time zoned in $^{29}Si/^{28}Si$ and $^{25}Mg/^{24}Mg$ because of the rapid rate of evaporation at high P_{H_2}.

An alternative hypothesis for CAI formation consistent with the Si and Mg isotope data presented here is exposure to numerous solar flare events. This would occur if CAIs formed in the inner annulus of the solar protoplanetary disk and were later dispersed to more distal regions of the disk, perhaps by x-winds [32,33]. The latter model predicts that CAIs formed in the reconnection ring of the solar protoplanetary disk where they were exposed to solar flares that occurred in cycles that persisted for perhaps tens of years [32]. As each individual solar flare event within an active cycle probably lasted for a few days, and CAIs are thought to be resident in the reconnection ring for on the order of 30 days, multiple melting events are implied. Our modeling of the Si and Mg isotope data suggests a maximum duration of melting of ~ 70 days at vacuum (or 15 days at a median temperature of 1773 K) and is consistent with residence of 144A in the reconnection ring region adjacent the protosun during active flaring. Melting by flares in the reconnection ring would likely occur at low gas pressures, suggesting that in this case the lack of Si and Mg isotope ratio zoning in the body of 144A is a primary feature and not the consequence of subsequent diffusive reequilibration.

The difference between the two scenarios described above is the P_{H_2} associated with melting, and assessment of the pressure attending melting of the CAI depends on the interpretation of the lack of substantial variation in $^{29}Si/^{28}Si$ and $^{25}Mg/^{24}Mg$ with radius across the object (excluding the margin, see below). If melting occurred at P_{H_2} greater than 10^{-6} bar (gas number density $= 4 \times 10^{12}$ cm^{-3}), as in a shock heating event or events, there would have been a significant curvature in the radial $\delta^{29}Si$ and $\delta^{25}Mg$ profiles in the CAI (Fig. 8). We showed above that elimination of this profile would require ~ 500 yr of exposure to high temperatures of ~ 1300 K. Centimeter-sized objects like CAIs are believed to have had a mean lifetime in the nebula of order 10^4 yr at heliocentric radii of 2 to 4 AU (and at total disk masses of 0.02–0.13 $M_{\odot}$) [34], and extensive subsolidus heating of CAIs for an integrated heating interval of hundreds of years spanning a total time interval (hot and cold intervals) of 300,000 yr in the protoplanetary disk has been proposed recently [11]. It appears that there was ample time for CAI 144A to have

experienced sufficient thermal processing to eliminate any Si and Mg isotope ratio gradients incurred during melting, if they existed. However, hundreds of years of subsolidus heating should have reset the ^{26}Al–^{26}Mg decay system early in the life of the CAI, implying that the initial ^{26}Al/^{27}Al recorded in this object should be below the initial for the solar system. This is not the case for 144A [11].

The alternative to subsolidus reequilibration is that P_{H_2} was less than 10^{-6} bar during melting (obviating the need for subsolidus reequilibration). In this case, multiple solar flare events are implied in so far as the gas pressures required to prevent isotopic zoning are thought to be too low to be consistent with shock heating.

Regardless of the thermobarometric history invoked to explain the lack of isotope ratio zoning in the body of 144A, subsolidus heating events subsequent to melting are required to explain the sharp gradients in Si and Mg isotope ratios at the margin of the object. The ~ 10 yr timescale obtained by modeling the profile as sublimation of the solid CAI is consistent with heating by numerous shock events or flares, or perhaps by passage into the inner nebula where ambient temperatures exceeded 1000 K [31].

The Si and Mg isotope ratio data for 144A require a minimum duration of post-melting thermal processing at high temperatures ($T > \sim 1300$ K) of ~ 10 to ~ 500 yr, depending upon the pressure attending melting.

8. Conclusions

Silicon LA-MC-ICPMS has been developed and applied to determine the astrophysical setting of formation of the CAI Leoville 144A. The new Si data combined with existing Mg isotope ratio data and models for the physical chemistry of evaporation place constraints on the time-pressure history of this CAI and, by extrapolation, other CAIs with similar Si and Mg isotope systematics. We find that the CAI was molten for a total of no more than 70 days and perhaps as little as a few hours, depending upon its subsequent history. Our results are consistent with melting either by exposure to a few shockwaves in the protoplanetary disk at $P_{H_2} \geq 10^{-6}$ bar or by exposure to numerous solar flare events like those envisaged in the x-wind model at much lower P_{H_2}. Each of these two scenarios has implications for the timescale of heating subsequent to melting. Shockwave heating requires hundreds of years of subsolidus heating to erase isotope zoning that would have been incurred during melting. Exposure to solar flares implies lower P_{H_2} during melting and obviates the need for hundreds of years of subsolidus heating. In

either case, years of sublimation of the solid CAI are required to explain the details of the Si and Mg isotope ratio profiles in the margin of the object. This work shows that combining Si and Mg isotope ratio data for CAIs yields constraints on the thermobarometric histories of CAIs and on the astrophysical setting of their melting.

Appendix A. Supplementary material

Supplementary data associated with this article can be found, in the online version, at doi:10.1016/j.epsl.2007.03.012.

References

[1] A. Galy, E.D. Young, R.D. Ash, R.K. O'Nions, The formation of chondrules at high gas pressures in the solar nebula, Science 290 (2000) 1751–1753.

[2] L. Grossman, D.S. Ebel, S.B. Simon, A.M. Davis, F.M. Richter, N.M. Parsad, Major element chemical and isotopic compositions of refractory inclusions in C3 chondrites: the separate roles of condensation and evaporation, Geochim. Cosmochim. Acta 64 (2000) 2879–2894.

[3] F.M. Richter, A.M. Davis, D.S. Ebel, A. Hashimoto, Elemental and isotopic fractionation of type B calcium–aluminum-rich inclusions: experiments, theoretical considerations, and constraints on their thermal evolution, Geochim. Cosmochim. Acta 66 (3) (2002) 521–540.

[4] R.N. Clayton, R.W. Hinton, A.M. Davis, Isotopic variations in the rock-forming elements in meteorites, Philos. Trans. R. Soc. Lond., A 325 (1988) 483–501.

[5] F.M. Richter, R.A. Mendybaev, A.M. Davis, Conditions in the protoplanetary disk as seen by the type B CAIs, Meteorit. Planet. Sci. 41 (2006) 83–93.

[6] T. Ding, D. Wan, R. Bai, Z. Zhang, Y. Shen, R. Meng, Silicon isotope abundance ratios and atomic weights of NBS-28 and other reference materials, Geochim. Cosmochim. Acta 69 (2005) 5487–5494.

[7] C. Molini-Velsko, T.K. Mayeda, R.N. Clayton, Isotopic composition of silicon in meteorites, Geochim. Cosmochim. Acta 50 (1986) 2719–2726.

[8] T. Ding, S. Jiang, D. Wan, Y. Li, J. Li, H. Song, Z. Liu, X. Yao, Silicon Isotope Geochemistry, 1996 125 pp., Beijing.

[9] C.B. Douthitt, The geochemistry of the stable isotopes of silicon, Geochim. Cosmochim. Acta 46 (1982) 1449–1458.

[10] E.D. Young, R.D. Ash, A. Galy, N.S. Belshaw, Mg isotope heterogeneity in the Allende meteorite measured by UV laser ablation-MC-ICPMS and comparisons with O isotopes, Geochim. Cosmochim. Acta 66 (4) (2002) 683–698.

[11] E.D. Young, J.I. Simon, A. Galy, S.S. Russell, E. Tonui, O. Lovera, Supra-canonical Al-26/Al-27 and the residence time of CAIs in the solar protoplanetary disk, Science 308 (5719) (2005) 223–227.

[12] E.D. Young, J.I. Simon, A. Galy, S.S. Russell, E. Tonui, O. Lovera, Supra-canonical Al-26/Al-27 and the residence time of CAIs in the solar protoplanetary disk, Science 308 (5719) (2005) Supplemental on-line material.

[13] E.D. Young, H. Nagahara, B.O. Mysen, D.M. Audet, Non-Rayleigh oxygen isotope fractionation by mineral evaporation: theory and experiments in the system SiO_2, Geochim. Cosmochim. Acta 62 (18) (1998) 3109–3116.

[14] E.D. Young, A. Galy, The isotope geochemistry and cosmochemistry of magnesium, in: geochemistry of non-traditional stable isotopes, Reviews in Mineralogy & Geochemistry, vol. 55, MSA, 2004, pp. 197–230.

[15] J.N. Cuzzi, C.M.O.D. Alexander, Chondrule formation in particle-rich nebular regions at least hundreds of kilometers across, Nature 441 (2006) 483–485.

[16] E.M. Stolper, Crystallization sequences of Ca–Al-rich inclusions from Allende: an experimental study, Geochim. Cosmochim. Acta 46 (1982) 2159–2180.

[17] P. Courtial, D.B. Dingwell, Densities of melts in the $CaO–MgO–Al_2O_3–SiO_2$ system, Am. Mineral. 84 (1999) 465–476.

[18] Y. Liang, F.M. Richter, B. Watson, Diffusion in silicate melts: II. Multicomponent diffusion in $CaO–Al_2O_3–SiO_2$ at 1500 °C and 1 GPa, Geochim. Cosmochim. Acta 60 (1996) 5021–5035.

[19] V.C. Kress, M.S. Ghiorso, Multicomponent diffusion in $MgO–Al_2O_3–SiO_2$ and $CaO–MgO–Al_2O_3–SiO_2$ melts, Geochim. Cosmochim. Acta 57 (1993) 4453–4466.

[20] E.D. Young, Assessing the implications of K isotope cosmochemistry for evaporation in the preplanetary solar nebula, Earth Planet. Sci. Lett. 183 (1–2) (2000) 321–333.

[21] F.M. Richter, A.M. Davis, D.J. DePaolo, B. Watson, Isotope fractionation by chemical diffusion between molten basalt and rhyolite, Geochim. Cosmochim. Acta 67 (2003) 3905–3923.

[22] P.E. Janney, F.M. Richter, A.M. Davis, R.A. Mendybaev, M. Wadhwa, Silicon isotope ratio variations in CAI evaporation residues measured by laser ablation multicollector ICPMS, Lunar and Planetary Science Conference, vol. XXXVI, 2005, p. 2123.

[23] H. Nagahara, K. Ozawa, Evaporation of forsterite in H_2 gas, Geochim. Cosmochim. Acta 60 (1996) 1445–1459.

[24] J.I. Simon, E.D. Young, S.S. Russell, E.K. Tonui, K.A. Dyl, C.E. Manning, A short timescale for changing oxygen fugacity in the solar nebula revealed by high-resolution ^{26}Al–^{26}Mg dating of CAI rims, Earth Planet. Sci. Lett. 238 (3–4) (2005) 272–283.

[25] E.D. Young, S.S. Russell, R.D. Ash, Ultraviolet laer ablation measurements of oxygen isotope ratios in a Leoville compact type A CAI, Lunar and Planetary Science Conference, vol. XXXI, 2000, p. 1873, abstr.

[26] E.M. Stolper, J.M. Paque, Crystallization sequences of Ca–Al-rich inclusions from Allende: the effects of cooling rate and maximum temperature, Geochim. Cosmochim. Acta 50 (1986) 1785–1806.

[27] H.S. Carslaw, J.C. Jaeger, Conduction of Heat in Solids, Oxford University Press, New York, 1959 510 pp.

[28] M. Morioka, H. Nagasawa, Diffusion in single crystals of melilite: II. Cations, Geochim. Cosmochim. Acta 55 (1991) 751–759.

[29] A.M. Davis, A. Hashimoto, R.N. Clayton, T.K. Mayeda, Isotope mass fractionation during evaporation of Mg_2SiO_4, Nature 347 (1990) 655–658.

[30] S.J. Desch, H.C. Connolly, A model of the thermal processing of particles in solar nebula shocks: Applications to the cooling rate of chondrules, Meteoritics 37 (2002) 183–202.

[31] A.P. Boss, Evolution of the solar nebula III. Protoplanetary disks undergoing mass accretion, Astrophys. J. 469 (1996) 906–920.

[32] F.H. Shu, H. Shang, M. Gounelle, A.F. Glassgold, T. Lee, The origin of chondrules and refractory inclusions in chondritic meteorites, Astrophys. J. 548 (2001) 1029–1050.

[33] F.H. Shu, H. Shang, T. Lee, Toward an astrophysical theory of chondrites, Science 271 (1996) 1545–1552.

[34] S.J. Weidenschilling, Radial drift of particles in the solar nebula: implications for planetesimal formation, Icarus 165 (2003) 438–442.